

Target Detection in Joint Frequency Modulated Continuous Wave (FMCW) Radar-Communication System

Saumya Dwivedi, Andre Noll Barreto, Padmanava Sen, and Gerhard Fettweis

Barkhausen Institut gGmbH, c/o TU Dresden, 01062 Dresden, Germany

Email: {saumya.dwivedi, andre.nollbarreto, padmanava.sen}@barkhauseninstitut.org,
Gerhard.Fettweis@tu-dresden.de

Abstract—Motivated by the need of combining hardware, energy and spectrum resources of various components towards developing autonomous vehicular systems, we propose a joint FMCW radar and communication (RadCom) system. The proposed waveform consists of frequency-modulated chirps, used for both radar and communications. Target detection is done using an FFT-based procedure. In contrast to the conventional FMCW-radar receiver, we have considered a short chirp duration to increase the data rate, resulting in a challenging scenario with non-negligible frequency components after mixing, corresponding to the transition between successive chirp symbols. For this scenario we obtained a closed-form analytic solution for detection and false-alarm probabilities, and simulated the communication system performance using a non-coherent receiver. Finally, simulation results are presented to demonstrate the performance of target detection and communication symbol decoding for the proposed joint RadCom system.

I. INTRODUCTION

Recently, there has been an increased interest in joint radar-communication (RadCom) systems [1]–[4], in which the same spectrum and waveforms are employed, both to transmit data and to detect objects in the propagation path using radar techniques. This is particularly relevant for autonomous vehicles, in which the detection of objects is necessary, and, at the same time, communication among different vehicles as well as with the infrastructure can help to coordinate traffic [5], [6]. Using the same signal for both purposes, one can efficiently use the available hardware, energy and spectrum for these two different purposes [7]–[9].

Existing literature proposes new waveforms for the joint RadCom systems. For instance, [2] considers a joint frequency-division multiple access channel for both radar and communication systems. It uses FMCW radar technology to enhance the target detection performance, while using an IEEE 802.11p waveform for vehicular communication. However, the framework therein does not facilitate an efficient use of available hardware and spectrum resources of both systems [7]. For a simultaneous RadCom operation, [3] proposes a joint IEEE 802.11ad-based waveform, in which only the preambles are used for radar sensing, resulting in lower target detection performance in comparison to employing full waveform.

This research was co-financed with tax money based on the budget approved by the delegates of the state parliament of Saxony, Germany.

Also, they consider a full-duplex radar and communication receiver system, which requires a complex receiver with self-interference cancellation. Another efficient way for a joint RadCom system to coexist is to use a time division duplex (TDD) mode between them. In this context, [4] considers pulse position modulation for embedding communication symbols with the radar symbols. However, the transceiver of the pulsed radar systems also operates in TDD mode, increasing the time for radar sensing, and leaving less time for communication symbol transmissions. On the other hand, [5] proposes a phase modulated continuous wave joint RadCom system with a direct sequence spread-spectrum technique. However, the complexity of the despreading receiver with large code sequences poses a major limitation for the design of power-constrained low-complexity vehicular systems. A recent work [6] employs orthogonal frequency division multiplexing (OFDM) for joint RadCom system. However, similarly to [3], it uses only the preambles for target detection.

This work proposes a joint FMCW RadCom system, which allows a relatively low cost, low-power implementation of chirp spread spectrum for communication [10], together with the popular FMCW radar systems for automotive applications [11]. We compare the performance of the radar receiver of the proposed RadCom system, either using the full transmit waveform or using only a preamble. Furthermore, conventional FMCW radar systems [11]–[13] assume either chirps with duration significantly longer than the reflection delay or the presence of guard bands between successive chirps, thereby ignoring the effect of the frequency components at the transition between symbols. However, these assumptions result in transmitting a significantly lower number of communication symbols per frame, reducing the data rate. Also, the latter assumption reduces the effective radar sensing time, resulting in poor target detection performance. Finally, the FFT-based target detection and distance estimation framework for FMCW radar receiver together with the non-coherent symbol decoder for the proposed frequency shift keying (FSK)-based chirp waveform are presented.

II. JOINT RADCOM SYSTEM MODEL

This section formulates the proposed joint FMCW RadCom system. The proposed system transmits a joint chirp-based waveform for both communication and radar systems, thus

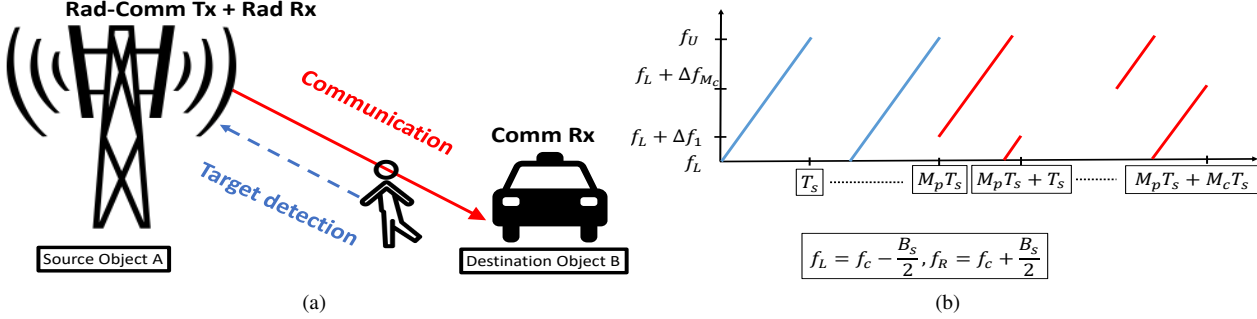


Fig. 1. (a) Joint RadCom system with source object A transmitting a joint waveform to detect the absence/ presence of a target as well as to communicate with destination object B . (b) Time-frequency response of the transmitted signal $x(t)$ with M_p number of preambles and M_c number of communication chirp- M -array FSK symbols such that the frequency shifts $\Delta f_j \in \{\Delta f^{(m)}\}_{m=1}^M$ where $1 \leq j \leq M_c$.

leveraging the benefits of spectrum reuse via simultaneous transmissions. Also, the communication links operate in TDD mode. Consider an application scenario as shown in Fig. 1(a), where a source object A transmits a joint waveform to detect the absence/ presence of a target as well as to communicate with destination object B . The joint RadCom transmitter model is presented below.

Let M_p unmodulated chirp symbols form the preamble part of a frame and M_c modulated chirp symbols be used for communication. Fig. 1(b) represents the time-frequency response of the transmitted waveform employing a chirp-based M -ary FSK (chirp- M -FSK) modulation. The mathematical representation of the proposed transmit waveform is formulated next. Firstly, the complex continuous time representation $s_i(t)$, $1 \leq i \leq M_p$, of the i -th chirp symbol during the preamble phase is given as

$$s_i(t) = \exp\left(i2\pi\left(f_c - \frac{B_s}{2}\right)t + i\pi S t^2\right), (i-1)T_s < t \leq iT_s, \quad (1)$$

where f_c denotes the carrier frequency, B_s and T_s represent the sweep bandwidth and symbol duration of the chirp waveform, respectively. Thus, the resulting positive slope S of the chirp signal is $S = \frac{B_s}{T_s}$. The chirp symbol duration is chosen to satisfy the condition $T_s = T_{\max}^d$ where $T_{\max}^d = \frac{2D_{\max}}{c}$ denotes the maximum target delay corresponding to the maximum target distance D_{\max} . Employing the chirp-based M -ary FSK (chirp- M -FSK) modulation for transmitting M_c communication symbols, the corresponding m -th, $1 \leq m \leq M$, modulated symbol $s^{(m)}(t)$ is given as

$$s^{(m)}(t) = \exp\left(i2\pi\left(f_c - \frac{B_s}{2}\right)t + i2\pi\Delta f^{(m)}t + i\pi S t^2\right), \\ 0 < t \leq \frac{B_s - \Delta f^{(m)}}{B_s} T_s \\ + \exp\left(i2\pi\left(f_c - \frac{B_s}{2}\right)t + i\pi S t^2\right), \frac{B_s - \Delta f^{(m)}}{B_s} T_s < t \leq T_s, \quad (2)$$

where $\Delta f^{(m)}$ denotes the frequency shift of the m -th symbol. The aggregate transmit signal per frame is given as

$$x(t) = \underbrace{\sum_{i=1}^{M_p} s_i(t)}_{x_p(t)} + \underbrace{\sum_{j=1}^{M_c} \tilde{s}_j(t)}_{x_c(t)}, \quad (3)$$

where $\tilde{s}_j(t) \in \{s^{(m)}(t - (j-1)T_s - M_p T_s)\}_{m=1}^M$ and $x_p(t)$, $x_c(t)$ denotes the transmitted symbol during the preamble and communication phase respectively. The radar and communication received signal models are developed next.

Let α_r denote the complex channel attenuation between the RadCom transmitter and target, on the distance d . Considering the scenario in Fig. 1(a), with stationary source object A and slow-moving target, the effect of Doppler shift can be ignored. Thus, the radar received signal is given as

$$y_{rad}(t) = \alpha_r x(t - t_d) + w_{rad}(t), \quad (4)$$

where $t_d = \frac{2d}{c}$ denotes the target delay and $w_{rad}(t)$ denotes the radar channel noise. The communication received signal $y_{com}(t)$ can be modeled as

$$y_{com}(t) = \exp(i\omega t) \alpha_c x(t) + w_{com}(t), \quad (5)$$

where α_c is the complex communication channel gain, ω is the angular Doppler frequency of the moving destination object B and $w_{com}(t)$ denotes the communication channel noise.

III. JOINT RADCOM TARGET DETECTION

This section develops the target detection framework for the joint RadCom system as follows. Let $\tilde{z}_p(t)$, $t_d < t \leq M_p T_s + t_d$ denote the signal obtained after analog mixing the radar received signal $y_{rad}(t)$ with the transmitted signal $x_p(t)$ during preamble phase followed by low pass filter and is given as $\tilde{z}_p(t) = \sum_{i=1}^{M_p} z_p^i(t)$, where the quantity $z_p^i(t)$ is

$$\tilde{z}_p^i(t) = \frac{1}{2} \alpha_r \exp(i2\pi S t_d t), (i-1)T_s + t_d < t \leq iT_s \\ + \frac{1}{2} \alpha_r \exp(i2\pi(B_s - S t_d)t), iT_s < t \leq iT_s + t_d \quad (6)$$

The second term in the expression above arises due to the consideration of $T_s = T_{\max}^d$, which is assumed to be negligible in the conventional FMCW radar systems [11]–[13]. Therefore, we aim to analyze the effect of FFT-based target detection and distance estimation framework for FMCW radar receiver with $T_s = T_{\max}^d$.

Let $\tilde{z}_p(n), 0 \leq n \leq M_p N - 1$, denotes the discrete time domain signal of $\tilde{z}_p(t)$, where $N = \frac{T_s}{T_{sam}}$ represents the number of samples per symbol with sampling duration T_{sam} . Thus, the target detection problem at the radar receiver of the source object A can be formulated in terms of the binary hypothesis testing framework as shown below

$$\begin{aligned} \mathcal{H}_0 : z_p(n) &= v_{rad}(n), \\ \mathcal{H}_1 : z_p(n) &= \tilde{z}_p(n) + v_{rad}(n), \end{aligned} \quad (7)$$

where $v_{rad}(n)$ denotes zero-mean complex Gaussian noise with variance σ^2 . Also, the hypotheses $\mathcal{H}_0, \mathcal{H}_1$ corresponds to the received signal in absence, presence of target, respectively. The model above assumes that the noise after analog mixing followed by low pass filtering is dominant. Also, the distance between the source and destination objects is known and hence the echo from destination object can be filtered out. Let, $Z_p(k), 1 \leq k \leq K$, denotes the periodogram of time domain symbols $z_p(n)$ with K representing the number of FFT bins in the frequency range $(0, B_s)$ and is given as

$$Z_p(k) = \frac{1}{K} \left| \sum_{n=0}^{M_p N - 1} z_p(n) \exp(-i2\pi k \frac{n}{M_p N}) \right|^2. \quad (8)$$

Thus, following a classical FFT-based FMCW radar detection framework [11]–[13], the joint target detection and distance estimation scheme is given as

$$\mathcal{T}_1 = \max_k Z_p(k) \underset{\mathcal{H}_0}{\overset{\mathcal{H}_1}{\geq}} \gamma, \quad (9)$$

$$\hat{f} = \frac{1}{T_{sam}} \arg \max_k Z_p(k), \quad (10)$$

where γ denotes the detection threshold and \hat{f} is the estimate of the target frequency $f = St_d = S \frac{2d}{c}$. Therefore, the estimated target distance \hat{d} is obtained as $\hat{d} = \frac{\hat{f}c}{2S}$. It can be seen from (6), that for the target lying close to the distance $\frac{D_{max}}{2}$, the peaks obtained at the frequencies St_d and $B_s - St_d$ are similar. Therefore, the following modified approach could be employed for improved radar detection performance in such scenarios.

$$\mathcal{T}_2 = \max_{\tilde{k}} \left(Z_p(\tilde{k}) + \bar{Z}_p(\tilde{k}) \right) \underset{\mathcal{H}_0}{\overset{\mathcal{H}_1}{\geq}} \gamma, \quad (11)$$

where $1 \leq \tilde{k} \leq \frac{K}{2}$ represent the FFT bins in the frequency range $(0, \frac{B_s}{2})$ and $\bar{Z}_p(\tilde{k}) = Z_p(K - \tilde{k})$ denotes the folded periodogram.

Remark: The target detection procedure above can be extended to the scenario where one can employ the communication symbols $x_c(t)$, in addition to the preamble symbols $x_p(t)$. Let, $\tilde{z}_f(n)$ denotes the discrete time domain representation of the low-pass filtered output of the mixed signal $x^*(t)y_{rad}(t), 0 < t \leq (M_p + M_c)T_s$. Therefore, the corresponding FFT-based detectors in (9), (11) for this scenario are modified as

$$\tilde{\mathcal{T}}_1 = \max_k Z_f(k) \underset{\mathcal{H}_0}{\overset{\mathcal{H}_1}{\geq}} \gamma, \quad (12)$$

$$\tilde{\mathcal{T}}_2 = \max_{\tilde{k}} \left(Z_f(\tilde{k}) + \bar{Z}_f(\tilde{k}) \right) \underset{\mathcal{H}_0}{\overset{\mathcal{H}_1}{\geq}} \gamma, \quad (13)$$

respectively, where $Z_f(k)$ is computed similar to (8) with total number of samples $(M_p + M_c)N$ and $z_f(n) = \tilde{z}_f(n) + v_{rad}(n)$ in lieu of $z_p(n)$, under \mathcal{H}_1 . Also, $\bar{Z}_f(\tilde{k})$ is computed as $\bar{Z}_f(\tilde{k}) = Z_f(K - \tilde{k})$.

The theoretical characterization of the detectors above in terms of probabilities of detection (P_D) and false-alarm (P_{FA}) as well as the procedure to obtain the corresponding detection threshold γ is obtained below.

A. Radar Performance Metrics

Let us define the probability metrics P_{FA}, P_D as [14]

$$P_{FA} = Pr(\mathcal{T}_l > \gamma; \mathcal{H}_0), \quad P_D = Pr(\mathcal{T}_l > \gamma; \mathcal{H}_1), \quad (14)$$

where $l \in \{1, 2\}$ for the detectors in (9), (11), respectively. Similar definition holds for the detectors in (12), (13) with $\tilde{\mathcal{T}}_l$ in lieu of \mathcal{T}_l . The lemma below presents the analytical expressions for P_{FA}, P_D corresponding to the detector in (9), while also deriving the detection threshold γ for the same.

Lemma 1. The P_{FA}, P_D for the detector in (9) is given as

$$P_{FA} = 1 - \left(1 - Q_{\chi_2^2} \left(\frac{2}{\sigma^2} \gamma \right) \right)^K, \quad (15)$$

$$P_D = 1 - \prod_{k=1}^K \left(1 - Q_{\chi_2'^2(\lambda_k)} \left(\frac{2}{\sigma^2} \gamma \right) \right), \quad (16)$$

where $Q_{\chi_2^2}$ and $Q_{\chi_2'^2(\lambda_k)}$ denote the complementary cumulative distribution function (ccdf) of central and non-central chi-square χ_2^2 random variable with 2 degrees of freedom. Also, the non-centrality parameter λ_k above is determined as

$$\lambda_k = \frac{1}{K} \left| \sum_{n=0}^{M_p N - 1} \tilde{z}_{pre}(n) \exp \left(-i2\pi k \frac{n}{M_p N} \right) \right|^2, \quad (17)$$

where $z_{pre}(n)$ is obtained using (6). Further, the detection threshold γ for a given P_{FA} is given as

$$\gamma = \frac{\sigma^2}{2} Q_{\chi_2^2}^{-1} \left(1 - (1 - P_{fa})^{\frac{1}{K}} \right), \quad (18)$$

where $Q_{\chi_2^2}^{-1}$ denotes the inverse of $Q_{\chi_2^2}$.

Proof. Given in Appendix. \square

On similar lines, the probability metrics P_{FA}, P_D for the detector in (11), are given as

$$P_{FA} = 1 - \left(1 - Q_{\chi_4^2} \left(\frac{2}{\sigma^2} \gamma \right) \right)^{\frac{K}{2}}, \quad (19)$$

$$P_D = 1 - \prod_{k=1}^{\frac{K}{2}} \left(1 - Q_{\chi_4'^2(\lambda_k)} \left(\frac{2}{\sigma^2} \gamma \right) \right), \quad (20)$$

where 4 degrees of freedom occur due to the fact that each of the real and imaginary components of the random variables $Z_{pre}(\tilde{k}), \bar{Z}_{pre}(\tilde{k})$ are independent $\chi_2^2, \chi_2'^2(\lambda_k)$ under hypotheses $\mathcal{H}_0, \mathcal{H}_1$, respectively. Subsequently, the corresponding P_{FA} expressions for the detectors in (12), (13), are identical to (15), (19), respectively. However, the corresponding P_D expressions are obtained similar to (16), (20), with the modified non-centrality parameter λ_k given as the statistical expectation of the quantity in (18), with $\tilde{z}_{full}(n)$ in lieu of $\tilde{z}_{pre}(n)$.

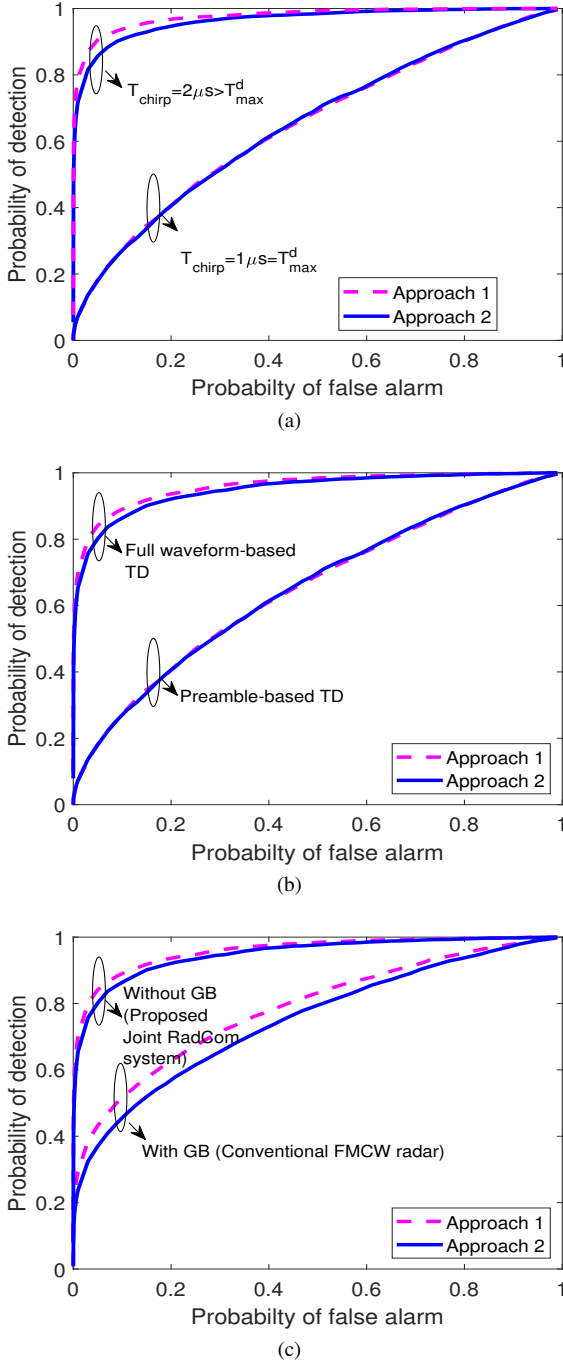


Fig. 2. Target detection (TD) performance comparison ($M = 16$, $\text{SNR}_{rad} = -19\text{dB}$): (a) With varying chirp duration T_s i.e. $T_s = T_{max}^d = 1\mu\text{s}$ and $T_s > T_{max}^d = 2\mu\text{s}$ for the preamble-based joint RadCom system. (b) With the preamble-based and full waveform-based joint RadCom system considering detectors in (9), (12) as Approach 1 and (11), (13) as Approach 2. (c) With the conventional FMCW radar receiver considering guard bands (GB) between successive chirp symbols and proposed joint RadCom system without GB employing full waveform-based TD.

IV. COMMUNICATION SYMBOL DECODING

In this section we use the communication receiver architecture at the destination object B similar to the optimum non-coherent FSK receiver for the frequency shift $\Delta f^{(m)} = \frac{m}{T_s}$ [15] as follows. The Doppler frequency ω of the moving destination object B is known at its communication receiver. Therefore, after defining $\tilde{y}_{com}(t)$ as $\tilde{y}_{com}(t) = \exp(-\iota\omega t)y_{com}(t)$,

the corresponding estimate $\hat{s}_j(t)$ of the j -th chirp- M -FSK symbol $\tilde{s}_j(t)$ is given as

$$\hat{s}_j(t) = \arg \max_{s^{(m)}(t)} \left| \int_0^{T_s} \Re(s^{(m)}(t)) \Re(\tilde{y}_{com}(t - (j-1)T_s - M_p T_s)) \right|^2 + \left| \int_0^{T_s} \Im(s^{(m)}(t)) \Im(\tilde{y}_{com}(t - (j-1)T_s - M_p T_s)) \right|^2, \quad (21)$$

where $s^{(m)}(t)$ is defined in (2) and $\Re(\cdot)$, $\Im(\cdot)$ denote the real, imaginary components, respectively of the corresponding quantities. The orthogonality of the chirp- M -FSK waveforms can be analyzed similar to the work in [10] and is out of the scope of this paper. Also, the theoretical bit-error-rate (BER) expressions for the non-coherent receiver above are yet to be explored in literature and also as our future work. However, this paper presents the simulation-based BER analysis.

V. SIMULATION RESULTS

Simulation results are presented below to characterize the target detection and communication symbol decoding performance for the proposed joint RadCom system operating at the carrier frequency $f_c = 8\text{GHz}$. The sweep bandwidth is set as $B_s = 1\text{GHz}$. It is worth mentioning that the carrier frequency of the proposed joint RadCom system can be increased to $f_c = 79\text{GHz}$, thus suitable for utilizing the licensed $77\text{GHz} - 81\text{GHz}$ automotive radar band for communication. The maximum target distance is set as $D_{max} = 150\text{m}$ resulting in the maximum target delay $T_{max}^d = \frac{2D_{max}}{c} = 1\mu\text{s}$. The number of possible symbols M for chirp- M -FSK is set as 16 for Fig. 2 - Fig. 3(a), while it is varied to 2, 64, 128 in the remaining figures. The number of chirp symbols in preamble and data transmission phase are set as $M_p = 5$, $M_s = 10$, respectively per frame, while we consider transmission of 10^4 such independent frames. The target detection performance is analyzed for various unknown target distance d as specified in the plots. The chirp duration is set as $T_s = T_{max}^d = 1\mu\text{s}$, while it is also varied to $T_s > T_{max}^d = 2\mu\text{s}$ in Fig. 2(a) for comparison. The signal to noise ratio SNR_{rad} , SNR_{com} at the radar, communication receivers respectively specified in the respective plots are defined as $\text{SNR}_{rad} = \frac{\alpha_r^2}{\sigma^2}$, $\text{SNR}_{com} = \frac{E_b}{N_0}$ with E_b denoting the bit energy and N_0 noise density. The detectors $\mathcal{T}_1, \tilde{\mathcal{T}}_1$, in (9), (12), respectively, are labeled as ‘Approach 1’ and the detectors $\mathcal{T}_2, \tilde{\mathcal{T}}_2$, in (11), (13), respectively, are denoted as ‘Approach 2’ in the respective figures.

The target distance d for the plots in Fig. 2 is set as $d = 40\text{m}$, while SNR_{rad} is -19dB . Fig. 2(a) compares the target detection performance of the preamble-based joint RadCom system with varying chirp duration i.e. $T_s \in \{1, 2\}\mu\text{s}$. Thus, ‘Approach1’, ‘Approach2’ in the legends therein represent the detectors $\mathcal{T}_1, \tilde{\mathcal{T}}_1$ respectively. As expected the figure demonstrate a significantly improved target detection performance of the RadCom system with $T_s > T_{max}^d = 2\mu\text{s}$ in comparison to that of $T_s = T_{max}^d = 1\mu\text{s}$. This is on account of the longer correlation between the transmitted and received chirp signal which is typically the case with conventional FMCW radar systems [11]–[13]. However, this performance improvement comes at a cost of 50% lower spectral efficiency of the

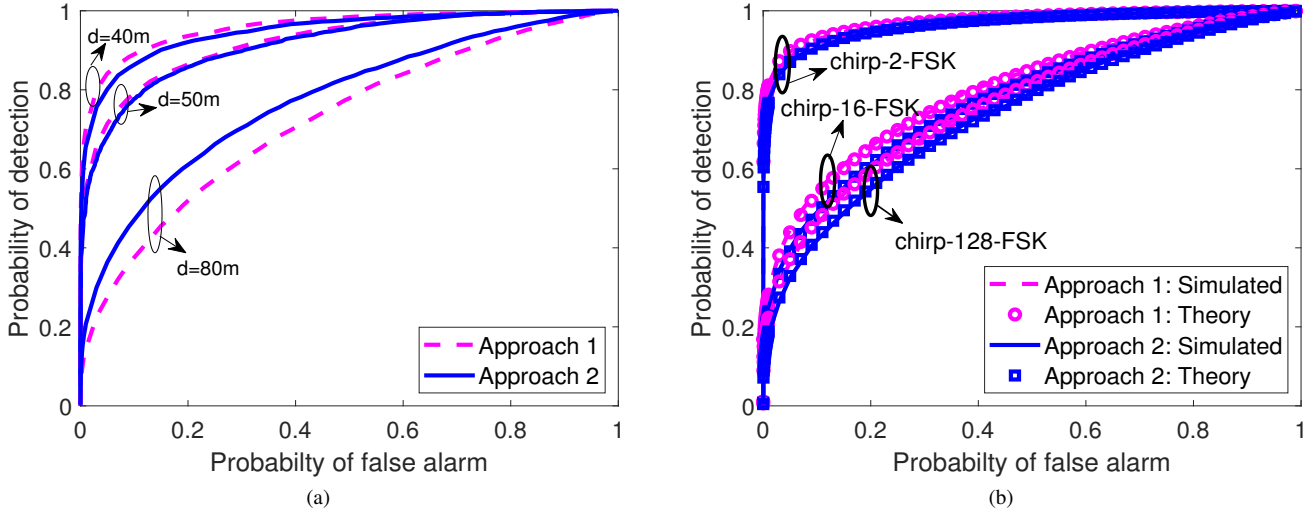


Fig. 3. Full waveform-based Target detection (TD) performance comparison: (a) With varying target distance d considering $M = 16$, $\text{SNR}_{rad} = -19\text{dB}$. (b) With varying M at $\text{SNR}_{rad} = -21\text{dB}$.

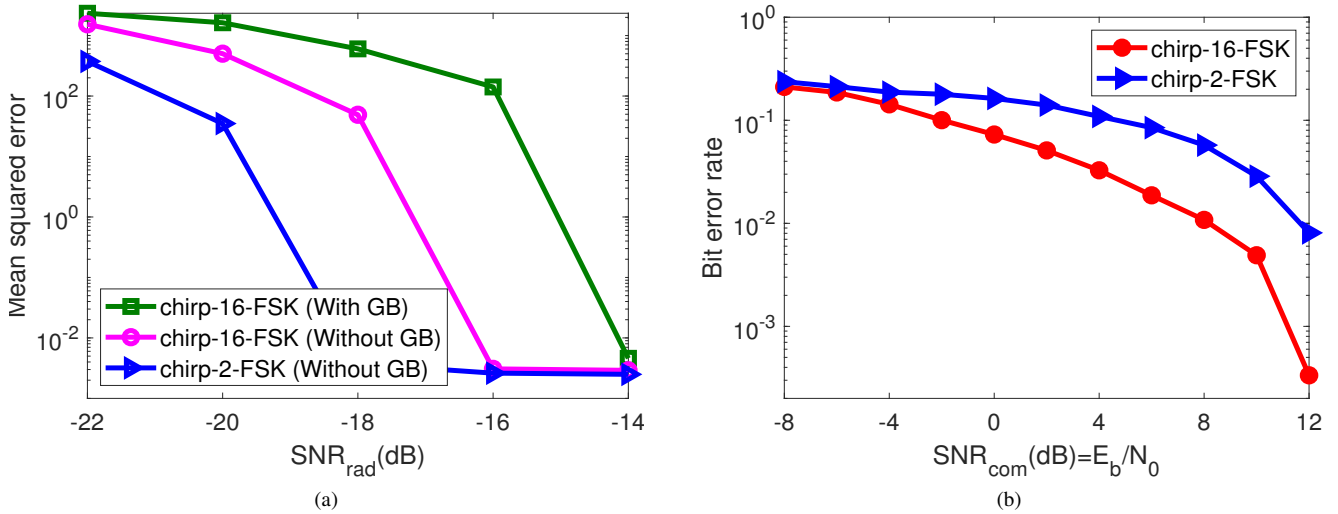


Fig. 4. Performance comparison with varying M : (a) MSE versus SNR_{rad} performance for the estimated target distance \hat{d} with $d = 40\text{m}$. (c) BER versus SNR_{com} performance for non-coherent chirp- M -FSK symbol decoder.

joint RadCom system. Thus, the subsequent figures considers $T_s = T_{max}^d$ and analyze the target detection performance for the various scenarios and approaches proposed in this work, that does not degrade its spectral efficiency.

Various plots in Fig. 2(b) for $T_s = T_{max}^d$ highlight the fact that the detectors $\tilde{T}_l, l \in \{1, 2\}$ representing the full waveform-based target detection achieve a significantly improved P_D for a given values of P_{FA} in comparison to the detectors \tilde{T}_l that consider the preamble-based target detection procedure. Further, both the detectors are seen to have the similar performance for the target distance $d = 40$. Owing to the significant performance improvement of the full waveform-based target detection procedure demonstrated herein, the subsequent simulation results for various scenarios are now presented for the the detectors \tilde{T}_1, \tilde{T}_2 , labeled as ‘Approach1’, ‘Approach2’, respectively. Fig. 2(c) demonstrates the significantly improved performance of the proposed joint RadCom system without guard bands (GB), with that of the conventional FMCW radar systems [11]–[13] considering GB between successive chirp

symbols $x(t)$.

Fig. 3(a) compares the performance of Approach 1, Approach 2, for varying target distance i.e. $d = 40\text{m}$, 50m , 80m . It shows that while both the detectors achieve similar P_D at given P_{FA} values for the target distances $d = 40\text{m}$, $d = 50\text{m}$. However, for the scenario with $d = 80\text{m} \approx \frac{D_{max}}{2}$, the Approach 2 improves the detection probability P_D in comparison to Approach 1 at a given P_{FA} . For instance, at $P_{FA} = 0.2$, Approach 2 achieves $P_D = 0.6$, while that of Approach 1 is $P_D = 0.5$. This is on account of the folding operation as can be seen in (13), which doubles the signal energy at the peaks obtained at target frequency for the scenario with $d \approx \frac{D_{max}}{2}$. The simulated as well as analytical target detection performances for Approach 1, Approach 2 at $\text{SNR}_{rad} = -21\text{dB}$ with varying $M = 2, 16, 128$ for a chirp- M -FSK symbols is presented in Fig. 3(b). It can be seen that on increasing M , the detection performance for the FMCW radar receiver employing the full-waveform based approach decreases. This is due to the presence of additional

number of peaks in the periodogram occurring at frequencies $St_d \pm (\Delta f^{(m)} - \Delta f^{(\tilde{m})})$, $B_s - St_d \pm (\Delta f^{(m)} - \Delta f^{(\tilde{m})})$. Also, the derived analytical expressions for the P_D , P_{FA} in section III-A are seen to fairly match with the simulated curves. It is worth mentioning that for the detectors in (9), (11), the effect of increasing M on the detection performance will be absent, since they depend only on symbols $x_p(t)$ for target detection instead of aggregate transmitted symbol $x(t)$.

Additionally, Fig. 4(a) plots the mean-squared estimation error i.e. $MSE = \mathbb{E} \left\{ (d - \hat{d})^2 \right\}$ versus SNR_{rad} for $M = 2, 16$, with $\hat{d} = \frac{\hat{f}_c}{2S}$ obtained using (10). It demonstrates the improved performance of the proposed system without guard bands (GB) with that of the conventional FMCW radar system with successive GB between the chirp symbols. Also, the lower MSEs are obtained with decreasing M , which draws similar inference as the detection plots in Fig. 3(b). The MSE curves are seen to saturate, since the true target frequency $f = S \frac{2d}{c}$ is present away from the the corresponding FFT bin boundary. Finally, the BER versus SNR_{com} analyses for the optimal non-coherent communication receiver in (21), with $M = 2, 16$, is shown in Fig. 4(b). It highlights the improved BER performance with increasing M . Thus, the cumulative results presented in Fig. Fig. 3(b)-Fig. 4, represent a trade off between the target detection and symbol decoding performances with the parameter M corresponding to the transmitted chirp- M -FSK symbols.

VI. CONCLUSION & FUTURE WORK

This paper proposes a RadCom system with joint transmit waveform comprising of chirp-based preambles and chirp- M -FSK-based communication symbols. The FFT-based target detection scheme at the radar receiver is developed along with the corresponding analytical results in terms of the probabilities P_D , P_{FA} . Also, the non-coherent chirp- M -FSK symbol decoder is presented. Simulation results demonstrate the significantly improved target detection and distance estimation performance of the proposed joint RadCom system with that of the conventional FMCW radar system which adds guard bands between successive chirp symbols. Further, for the scenario with target distance $d \approx \frac{D_{max}}{2}$, the modified FFT-based detection Approachrithm is presented, which results in improved performance. The results presented herein also demonstrate the improved target detection performance by using full transmit waveform than using only a preamble. Finally, the simulated BER analyses are obtained using the non-coherent chirp- M -FSK symbol decoder presented in this work. Future work will extend the proposed target detection framework for a joint RadCom multiple-input multiple-output (MIMO) system.

APPENDIX

PROOF OF LEMMA 1

It can be seen from (8), that the distributions of the quantity $\frac{2}{\sigma^2} Z_{pre}(k)$ under hypotheses $\mathcal{H}_0, \mathcal{H}_1$ are given as

$$\frac{2}{\sigma^2} Z_{pre}(k) \sim \begin{cases} \chi_2^2, & \mathcal{H}_0, \\ \chi_2^2(\lambda_k) & \mathcal{H}_1, \end{cases} \quad (22)$$

where the non-centrality parameter λ_k above is computed as the sum of absolute squares of the mean of Gaussian random variable $\frac{1}{K} \sum_{n=0}^{M_p N - 1} z_{pre}(n) \exp(-t2\pi k \frac{n}{M_p N})$, and can be obtained as given in (17). Employing (14), (22), one obtains

$$\begin{aligned} P_{FA} &= 1 - Pr \left(\max_k Z_{pre}(k) < \gamma; \mathcal{H}_0 \right) \\ &= 1 - \prod_{k=1}^K Pr \left(\frac{2}{\sigma^2} Z_{pre}(k) < \frac{2}{\sigma^2} \gamma; \mathcal{H}_0 \right), \\ P_D &= 1 - \prod_{k=1}^K Pr \left(\frac{2}{\sigma^2} Z_{pre}(k) < \frac{2}{\sigma^2} \gamma; \mathcal{H}_1 \right). \end{aligned}$$

Thus, resulting in the closed form expressions in (15), (16), respectively. Further, employing (15) for the P_{FA} , the detection threshold γ is obtained as given in (18).

REFERENCES

- [1] C. Sturm and W. Wiesbeck, "Waveform design and signal processing aspects for fusion of wireless communications and radar sensing," *Proceedings of the IEEE*, vol. 99, no. 7, pp. 1236–1259, 2011.
- [2] C. Aydogdu, N. Garcia, and H. Wymeersch, "Radar communication for combating mutual interference of FMCW radars," *arXiv preprint arXiv:1807.01497*, 2018.
- [3] P. Kumari, J. Choi, N. González-Prelcic, and R.W. Heath, "IEEE 802.11 ad-based radar: An approach to joint vehicular communication-radar system," *IEEE Trans. on Vehicular Technology*, vol. 67, no. 4, pp. 3012–3027, 2018.
- [4] M. Bocquet, C. Loyez, C. Lethien, N. Deparis, M. Heddebaut, A. Rivenq, and N. Rolland, "A multifunctional 60-GHz system for automotive applications with communication and positioning abilities based on time reversal," in *The 7th European Radar Conf. IEEE*, 2010.
- [5] S.H. Dokhanchi, M.R.B. Shankar, . Stifter, and B. Ottersten, "Multicarrier phase modulated continuous waveform for automotive joint radar-communication system," in *19th International Workshop on Signal Process. Advances in Wireless Comm. (SPAWC)*. IEEE, 2018.
- [6] S.H. Dokhanchi, B.S. Mysore, K.V. Mishra, and B. Ottersten, "A mmWave automotive joint radar-communications system," *IEEE Trans. on Aerospace and Electronic Systems*, 2019.
- [7] B. Paul, A.R. Chiriyath, and D.W. Bliss, "Survey of RF communications and sensing convergence research," *IEEE Access*, vol. 5, pp. 252–270, 2017.
- [8] J.G. Metcalf, C. Sahin, S.D. Blunt, and M. Rangaswamy, "Analysis of symbol-design strategies for intrapulse radar-embedded communications," *IEEE Trans. on Aerospace and Electronic Systems*, vol. 51, no. 4, pp. 2914–2931, 2015.
- [9] J. Choi, V. Va, N. Gonzalez-Prelcic, R. Daniels, C.R. Bhat, and R.W. Heath, "Millimeter-wave vehicular communication to support massive automotive sensing," *IEEE Comm. Magazine*, vol. 54, no. 12, pp. 160–167, 2016.
- [10] L. Vangelista, "Frequency shift chirp modulation: The LoRa modulation," *IEEE Signal Process. Letters*, vol. 24, no. 12, pp. 1818–1821, 2017.
- [11] S. M. Patole, M. Torlak, D. Wang, and M. Ali, "Automotive radars: A review of signal processing techniques," *IEEE Signal Process. Magazine*, vol. 34, no. 2, pp. 22–35, 2017.
- [12] F.M. Ahmed, K.A. Elbarbary, and A.R.H. Elbardawiny, "Analytical performance evaluation of an enhanced frequency domain radar detector," in *Radar Conf. IEEE*, 2008.
- [13] S. Neemat, O.A. Krasnov, and A. Yarovoy, "Simultaneous processing of time-shifted orthogonal LFM CW waveforms," in *Signal Processing Symposium (SPSymo)*. IEEE, 2017.
- [14] S. Kay, *Fundamentals of statistical processing: Detection theory*, vol. 2, Prentice Hall America, 1998.
- [15] J. Proakis and M. Salehi, *Digital communication, and linear modulation theory*, McGraw-Hill education, 2007.